

Electrical and optical properties of platinum doped titanium dioxide nanoparticle: improved performance in dye sensitized solar cells

OMAR A. AL-HARTOMY*

Physics Department, Faculty of Science, King Abdul Aziz University, Jeddah 21589, Saudi Arabia

The undoped and doped TiO₂ particles with different concentrations of Pt (1-6%) were synthesized by a simple hydrothermal method. The resulting material was further characterized by standard analytical techniques such as x-ray diffraction (XRD), scanning electron microscopy (SEM), and UV-vis spectroscopy. The XRD analysis showed no change in crystal structure of TiO₂ after doping with different concentration of Pt, confirming anatase phase of TiO₂. The electrical analysis showed that the dielectric constant (ϵ') and dielectric loss tangent ($\tan \delta$) had decrement trend with increase in frequency. The dielectric property was found to decrease with increase in dopant concentration. At low frequency, the mechanism of a.c. conductivity was found to be same as that of d.c. conduction. With increase in frequency, the magnitude of complex impedance was found to decrease indicating the increase in a.c conductivity. Dopant concentration was also found to increase with corresponding increase in the value of impedance. Under simulated solar illumination, the amount of dye absorption was found to increase with the increase in optimum content of Pt, resulting in the gradual increase in photovoltaic current, this could be contributed to the improvement in the cell efficiency from 6.45 to 7.62%.

(Received May 30, 2014; accepted May 7, 2015)

Keywords: Pt-doped TiO₂; Complex impedance; Dielectric properties; a.c. Conductivity

1. Introduction

Titanium dioxide (TiO₂) has attracted a lot of attention in the recent years due to its potential application in solar cell. Its wide band gap (3.2 eV), limits the use of visible light and only a small fraction not more than 5% of the solar spectrum is utilized in the advance oxidation process. Scientists working in this area have tried to modify the physical and chemical composition of TiO₂ by doping with metal/non-metals in order to enhance the catalytic property of TiO₂. The doping of TiO₂ with V, Cr, Mn, Fe, Ni, Cu, C, Co etc. has been reported earlier, employing different methodologies [1-4]. It is well known that UV irradiation requires high energy source and is costlier as well as hazardous [5], therefore, the use of visible light is preferred. It is also very interesting to study the electrical properties of synthesized TiO₂, the impedance spectroscopy is an effective method as it can resolve the grain and grain boundary contribution to the synthesized material [6]. TiO₂ has stable dielectric properties which are characterized by its high dielectric constant (or relative permittivity) and low dielectric loss [7]. Such materials have applications in micro communication system [8].

In particular, synthesis of Pt doped TiO₂ composite materials are reported in literature using different methodologies [9, 10, 11]. But systematic studies about its low cost synthesis and quest about other electrical properties relating to the improvement of photocatalytic properties under UV and visible region are absent. This study will also give a new perspective in the search of material suitable for enhancing the efficiency of solar cell.

2. Experimental details

2.1 Reagents and Chemicals

Titanium isopropoxide, 2-chlorophenol, cetyltrimethyl ammonium bromide hexachloro platonic acid and di-tetrabutyl ammonium cis-bis (isothiocyanato)bis(2,2'-bipyridyl-4,4'-dicarboxylato)ruthenium(II) (95%, N719 dye) were obtained from Sigma-Aldrich. Glacial acetic acid, sulfuric acid, triton X-100 and methyl orange were obtained from Merck.

2.2 Synthesis of undoped and Pt doped TiO₂ nanoparticle using the hydrothermal method

Titanium isopropoxide (1.5 g) in 2-propanol (50 mL) was mixed with 2 g surfactant (Triton X-100) in 100 mL of distilled water and then 1.5 g of concentrated sulfuric acid (95%) was added drop wise into the solution under vigorous magnetic stirring and the resultant mixture was kept at 50 °C for 10 h. Hydrothermal treatment was carried out at 180±1 °C for about 36 h. After cooling the solution to room temperature, the precipitate obtained was filtered out, washed with doubled distil water, dried in the air and then calcined at 400 ±1 °C (Only at this temperature, we get nanoparticles) for about 16 h in nitrogen atmosphere. For doping of TiO₂ particle with Pt a known concentration of hexachloroplatonic acid (1-6%, w/v) was added in the surfactant solution. For the analysis of electrical properties a pellet of 13 mm in diameter and of thickness 1.8 mm was made by applying pressure up to 7 ton/cm² on the powder sample.

2.3 Dye Sensitized Solar Cell (DSSC) Preparation

For DSSC preparation, the synthesized TiO₂ powder was mixed with dilute acetic acid (0.035M) and a few drops of Triton X-100 to make the soupy colloidal paste which was then applied as a thick film (40-50 nm) onto the conductive glass plates towards its conductive side. The plate was heated for 10 minutes, cooled down to room temperature and then placed in a beaker containing 0.5mM ethanol N719 solution. Another conductive plate was made as the positive counter electrode by depositing carbon (soot) on the conducting side. The sandwiching of the two plates (positive and negative electrodes) was offset and a solar simulator with a 500 W halogen lamp having a light intensity of 100mW/cm² was employed to illuminate the dye sensitized solar cells (DSSCs).

2.4 Apparatus

The structural characterization of undoped and doped TiO₂ nanoparticles was performed by XRD in the 2θ range of 20-80° (RigakuMiniflex II) with Cu Kα radiations (λ = 1.5418 Å) operated at a voltage of 30 kV and current of 15 mA. The UV-Vis spectra were recorded using Shimadzu UV-vis spectrophotometer (Model number-1601). The morphology and size were observed by SEM (Leo 435 VP). Electrical properties were measured using computer control LCR meter (measure frequency upto few GHz) analyzer (Model Agilent E4982A,). Photovoltaic properties were recorded using a digital multimeter (Keithley 2000).

3. Results and discussion

3.1 X-ray Diffraction:

The XRD pattern analysis of Pt-doped TiO₂ with different concentrations of Pt is shown in Fig. 1. Pt-doped TiO₂ showed no impurity peaks indicating products being in pure anatase phase. These results indicate that the phase structure remains unchanged during doping of Pt. The average anatase crystallite size of doped and undoped TiO₂ nanoparticles was determined by Scherrer's formula [12].

$$D = \frac{k\lambda}{\beta \cos \theta} \quad (1)$$

where D is the crystallite size, k the shape factor (a constant; in our case it is 0.9), λ the wavelength, θ the diffraction angle and β is the full width at half maximum (FWHM). Table 1 shows the mean size of the crystallites in samples which were estimated by the FWHM of the most intense XRD peak (101) using the Scherrer equation (1). It can be observed that the crystallite size was found to decrease up to certain limits (5.0 % Pt) and then remain almost constant with the increase in Pt concentration as a dopant. This could be explained on the basis of the fact

that the addition of dopant may hinder the growth of TiO₂ particle to some degree [10].

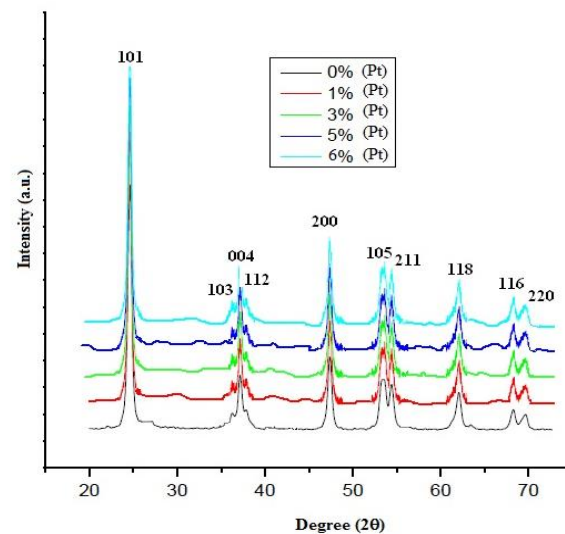


Fig. 1. XRD patterns of undoped and Pt-doped TiO₂. Calcination temp: 400±1 °C, calcination time: 16 h.

3.2 UV-Vis Absorption Spectra:

The UV-Vis absorption spectra of solution sample of undoped and Pt doped TiO₂ is shown in Fig. 2. The band gap energies of undoped and Pt doped TiO₂ particles with the obtained wavelength from UV-Vis absorption spectra were calculated using the following equation (2) [12] and the results are depicted in Table 1.

$$E_g = \frac{hc}{\lambda} \quad (2)$$

where h is the Planck's constant (6.634×10^{-34} Js) and c is the speed of light (3×10^8 m/s). A total number of 15 samples were analyzed here, 3 samples for each 5 different concentration of Pt. The overall results of analysis are shown in Table 1. As expected, incorporation of dopant (Pt) into TiO₂ lattice has been found to shift the fundamental absorption edge towards the longer wavelength i.e. red shift. [13]. It can be seen from the table that the crystallite size was found to decrease (from 11.2 nm to 7.4 nm) upto certain limits (5 % doping of Pt) and then increases (7.45 nm) with the increase in Pt concentration as a dopant. Further increase in dopant concentration leads to decrease in the band gap energy from 3.17eV to 2.93 eV (decrement is 7.57%) upto 5% dopant of Pt. This may be due to the deposition of the metal on the photocatalyst which covered the surface of TiO₂ and can reduce the effective surface area for absorbing light.

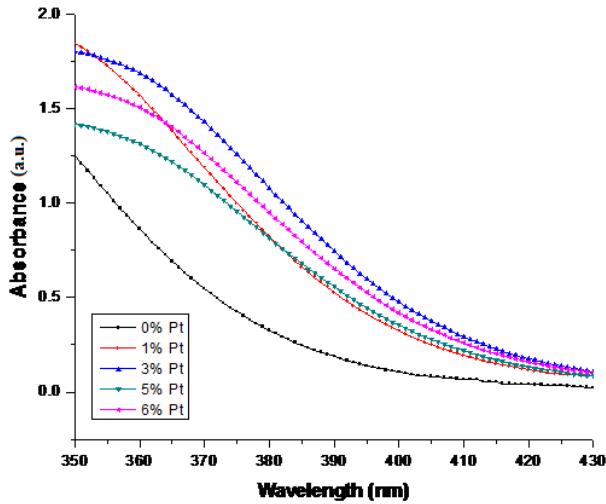


Fig. 2: Absorption spectra of undoped and Pt-doped TiO_2 . Calcination temp: $400 \pm 1^\circ\text{C}$, calcination time: 16 h.

Table 1. Crystallite size and Band gap energy of undoped and Pt-doped TiO_2 with different concentration of dopants. Calcination temp: 400°C , calcination time: 16 h.

S. No.	Pt concentration (%)	Crystallite size (nm)	Band gap (eV)
1.	0.0	11.2	3.17
2.	1.0	9.8	3.04
3.	3.0	8.2	2.96
4.	5.0	7.4	2.93
5.	6.0	7.45	2.95

3.3 Scanning electron microscopy

The microstructural characterization of undoped and Pt doped TiO_2 nanoparticles were carried out by scanning electron microscopy. The morphology of 5% Pt doped TiO_2 particles calcined at $400 \pm 1^\circ\text{C}$ for about 16 h are presented in Fig. 3. The SEM images of Pt doped TiO_2 at magnifications 5000X show the agglomerated spherical partial with crystalline nature and rough surfaces.

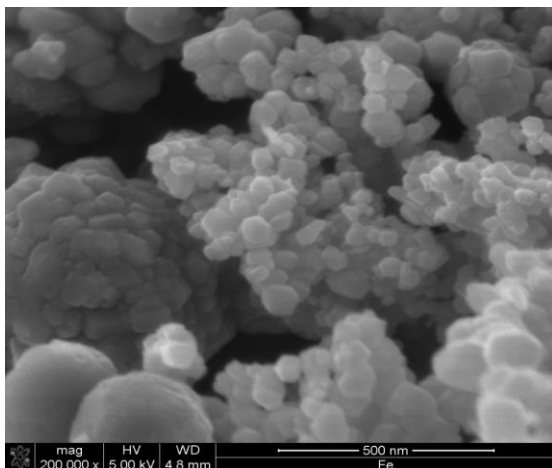


Fig. 3. SEM images of 5% Pt-doped. Calcination temp: $400 \pm 1^\circ\text{C}$, Calcination time: 16 h.

3.4 Electrical properties

3.4.1 Impedance Analysis

For impedance analysis, each semicircular arc can be fitted by an equivalent circuit having a resistor (R) and a capacitor (C) which are connected in parallel. The equivalent circuit consisting of a series of connected parallel resistance R and capacitance C elucidate the impedance spectra. The complex impedance is the sum of real and imaginary part, and is represented as:

$$Z^* = Z' + jZ'' \quad (3)$$

Where Z' and Z'' are given by the following relations

$$Z' = \frac{R_g}{1 + (\omega_g^2 C_g^2 R_g^2)} + \frac{R_{gb}}{1 + (\omega_{gb}^2 C_{gb}^2 R_{gb}^2)} \quad (4)$$

$$Z'' = \frac{R_g^2 \omega_g C_g}{1 + (\omega_g^2 C_g^2 R_g^2)} + \frac{R_{gb}^2 \omega_{gb} C_{gb}}{1 + (\omega_{gb}^2 C_{gb}^2 R_{gb}^2)} \quad (5)$$

Where R_g , R_{gb} , C_g , and C_{gb} are the resistance and capacitance of the grain and grain boundary, respectively, while ω_g and ω_{gb} are the frequencies at the peaks of the semicircles for grain and grain boundary, respectively.

Figs. 4 and 5 show the real part (Z') and imaginary part (Z'') of impedance with frequency at different concentration of undoped and Pt doped TiO_2 respectively, which shows that Z' and Z'' decreases with increase in frequency due to the space charge contribution [14]. At low frequency the complex impedance values are higher which indicate the larger polarization, which on further increase in frequency shows independent behaviour.

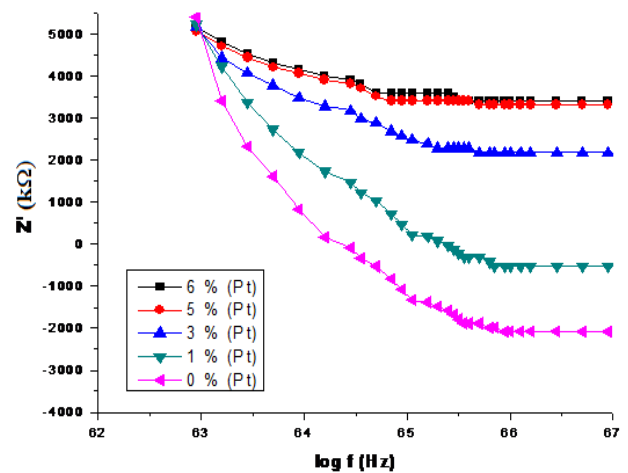


Fig. 4. Variation in real impedance Z' as a function of frequency and compositions.

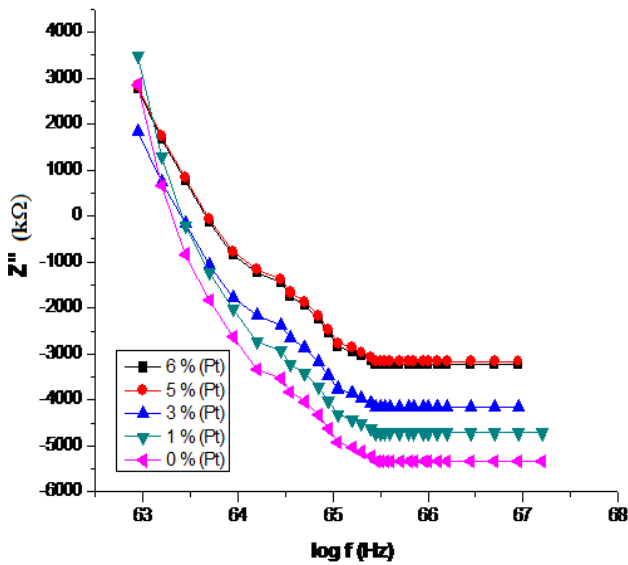


Fig. 5: Variation in imaginary impedance Z'' with frequency.

3.4.2 Dielectric Studies

In order to find the material suitable for high frequency microelectronic device application dielectric studies have been carried out. The variation of tangent loss ($\tan \delta$) and dielectric constant (ϵ') with frequency for various concentration of undoped and Pt doped TiO_2 are shown in Figs. 6 and 7, respectively, at room temperature. At low frequency, the dielectric constant is high due to the accumulation of charges at the grain boundary, and at the interface of sample and electrode [15]. As the frequency increases, the dielectric constant decreases due to the gradual diminishing of the space charge polarization indicating the electronic and atomic contribution domination. The dielectric constant is independent at higher frequency which indicates the domination of electronic and atomic contribution [16].

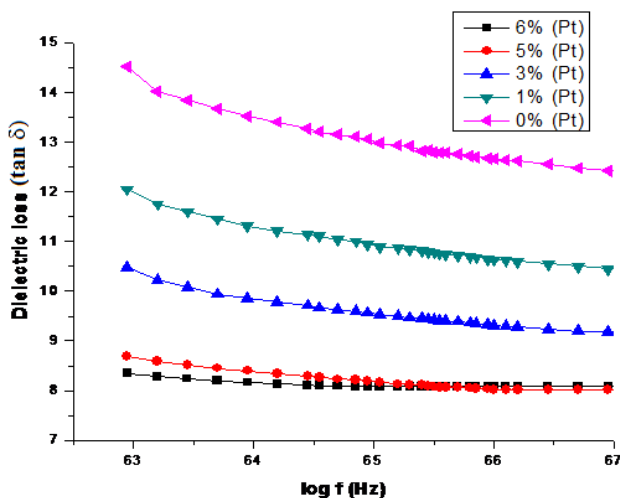


Fig. 6: Variation in dielectric loss with frequency at different compositions.

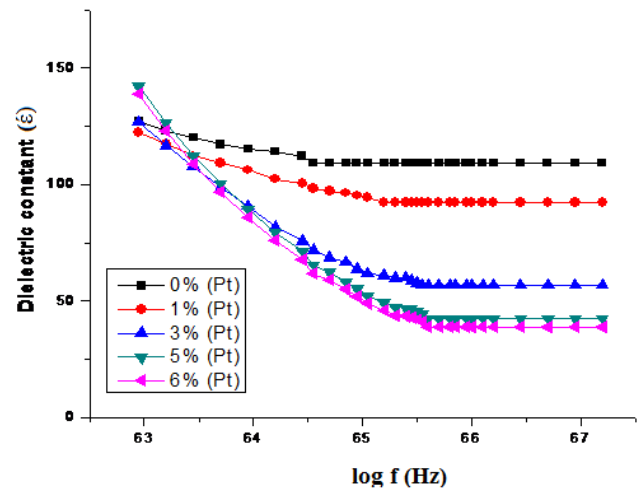


Fig. 7: Variation in dielectric constant with frequency for different compositions.

Another reason can be attributed on the basis of Maxwell–Wagner interfacial model [17]. According to this model, a dielectric medium consists of double layers having well conducting grains that are separated by poorly conducting grain boundaries. When the external electric field is applied, the charge carriers can easily migrate the grains, but they were accumulated at the grain boundaries resulting large polarization and high dielectric constant. The higher value of dielectric constant is also due to inhomogeneous dielectric structure which may be due to porosity and grain structure. The dielectric properties decrease with the increase in frequency and then show independent behaviour due to the fact that beyond a certain frequency of external field the hopping between metal ions cannot follow the alternating field.

3.4.3 a.c. Conductivity

Fig. 8 shows the variations of a.c conductivity with frequency for undoped and Pt doped TiO_2 at room temperature. The overall conductivity is the sum of a.c. conductivity and d.c. conductivity, which is given by

$$\sigma = \sigma_o(T) + \omega \epsilon_o \epsilon_r \tan \delta \quad (6)$$

Where ω is the angular frequency, and ϵ_o is the permittivity of free space, $\sigma_o(T)$ is the d.c. conductivity, which is due to band conduction and independent of frequency whereas $\omega \epsilon_o \epsilon_r \tan \delta$ is the a.c. conductivity, which depends on frequency. The conductivity increases with the increase in frequency as the electron hopping frequency enhances [18]. It also shows that the a.c conductivity decreases with increase in dopant concentration due to the decrease in the particle size and increase in the ratio of the surface volume. Another reason can be attributed to the fact that the dopants can introduce the defect ions in TiO_2 lattice. These defects may lead to segregate at the grain boundaries due to the diffusion

process resulting from sintering and cooling processes. Therefore, on increasing the dopant concentration, the concentration of defect ions also increases, hence facilitates the formation of grain boundary defect barrier which may lead to the blockage of flow of charge carriers resulting the decreases in the conductivity of the system [15].

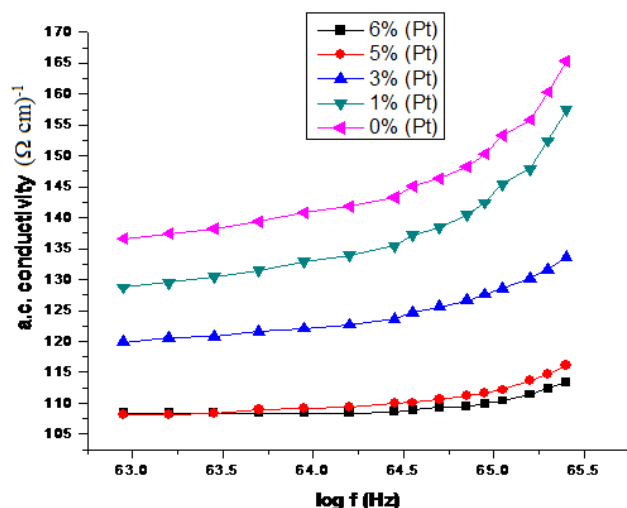


Fig. 8. Variation of a.c. conductivity with frequency for different compositions.

3.4.4 Photo-electric performance of DSSCs

The photo-voltaic performance of pure and Pt-doped TiO₂ electrode having different concentrations of Pt (1-6%) using N-719 dye was investigated and the results are incorporated in Fig. 9 and Table 2. The power conversion efficiency of the solar cell was determined by the following Eq:

$$\eta = Voc \times Jsc \times FF / Pin \times 100\% \quad (7)$$

Where Voc , Jsc , Pin represent the open-circuit photo voltage, the short-circuit photocurrent and the incident light power, respectively. Furthermore the fill factor was calculated by the following Eq:

$$FF = Vmax \times Jmax / Voc \times Jsc, \quad (8)$$

Where $Vmax$ and $Jmax$ represents the voltage and the current at the maximum output power.

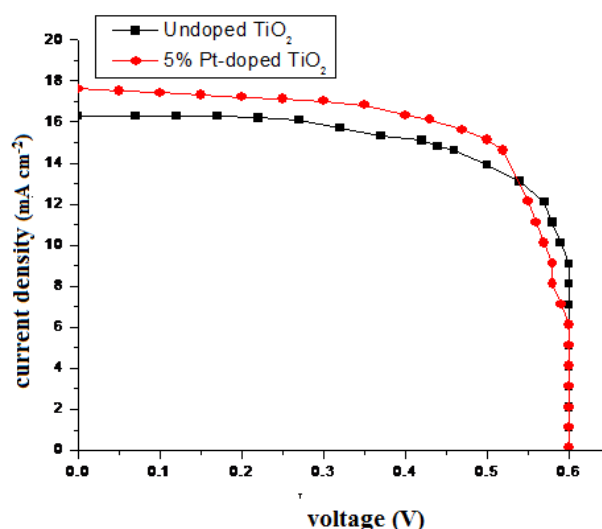


Fig. 9. Current–voltage (I – V) characteristics of solar cell with TiO₂ film containing 0% and 5% Pt doped TiO₂, measured at one sun illumination (100 mW cm^{-2} , AM 1.5).

Table 2: The photovoltaic parameters of DSSCs based on Pt-doped TiO₂ with different concentration of dopants.

Sample number	Dopant content (%)	Jsc (mA cm ⁻²)	Voc (V)	F.F (%)	Vmax Efficiency (%)
1	0	16.30	0.60	0.66	6.45
2	1	16.72	0.59	0.68	6.71
3	3	17.17	0.60	0.69	7.10
4	5	17.63	0.60	0.72	7.62
5	6	17.42	0.56	0.70	6.83

The result shows that Jsc , FF and Voc were higher in case of doped TiO₂ as compared with undoped TiO₂ working electrode. As the contents of Pt in TiO₂ film increased from 0 to 5%, the energy conversion efficiency of the DSSC was increased from 6.45 to 7.62 %. The Pt content involved in TiO₂ reduces the loss of electrons by suppressing their recombination, and this results in a significant increase in the short-circuit current and the overall power conversion efficiency.

4. Conclusions

Pt doped TiO₂ nano-particle was synthesised using hydrothermal technique. The doping of Pt into TiO₂ lattice shifts the position of its fundamental absorption edge towards the longer wavelength and reduces its band gap energy. The XRD analysis shows no change in crystal structure of TiO₂ after doping with different concentration of Pt indicating single phase polycrystalline material. The SEM analysis of doped TiO₂ shows the agglomerated

spherical partial having crystalline nature with rough surfaces. The dielectric constant of Pt doped TiO₂ decreases in the low frequency region with an increase in frequency, whereas in the high frequency region, it shows the frequency independent behaviour implying that the material is suitable for high frequency microelectronic device applications. The dielectric loss of Pt doped TiO₂ is constant at high frequency. The complex impedance of Pt doped TiO₂ decreases with increase in frequency resulting an increase in a.c. conductivity. The impedance increases with increase in dopant concentration in TiO₂ which in turn causes a corresponding decrease in a.c conductivity. In DSSCs Pt-doped TiO₂ possesses higher photocurrent due to a higher dye uptake and also reduces the loss of electrons by suppressing their recombination, as a result, a significant increase in the overall power conversion efficiency was observed.

References

- [1] M. M. Haque, A. Khan, K. Umar, Niyaz A. Mir, M. Muneer, T. Harada M. Matsumura. *Energy Environ. Focus* **2**, 73 (2013).
- [2] C. Cao, C. Hu, W. Shen, S. Wang, H. Liu, Jianli Wang.. *Sci. Adv. Mater.* **5**, 1256 (2013).
- [3] V. D. Binas, K. Sambani, T. Maggos, A. Katsanaki, G. Kiriakidis, *Appl. Catal. B: Environ.* **113-114**, 79 (2012).
- [4] G.L. Huang, M. Jani, Y.-L. Huang, W.-C.V. Yeh, *Sci., Adv. Mater.* **5**, 1444 (2013).
- [5] M. Muruganandham, M. Swaminathan. *Sol. Energ. Mat. Sol. C.*, **81**, 439 (2004).
- [6] A. Azam, A.S. Ahmad, M. Chaman, A.H. Naqvi. *J. Appl. Phys.* **108**, 1 (2010).
- [7] M.H. Mangrola, B.H. Parmar, A.S. Pillai, V.S. Joshi. *Multi Disciplinary edu global quest.* **1**, 138 (2012).
- [8] T. Fuyuki, H. Matsunmi. *Jpn. J. Appl. Phys.* **25**, 1288 (1986).
- [9] H. Song, T Chen, Sun Ya Li, Zhung Xue-Qiang, Jia Xio-hua.. *Ceram Int.* **40**, 11015 (2014).
- [10] Jinghua Cai, Z. Wang, L. Kangie, Yang Zheng, Jiaguo Yu, Mei Li. *RSC adv.* **3**, 15273 (2013).
- [11] Tianou He, Xiaoling Guo, Kui Zhang, Yaming Feng, Xiangdong Wang. *RSC adv.* **4**, 5880 (2014).
- [12] D. Mardare, G.I. Rasu, *J. Optoelectron. Adv. Mater.*, **6**, 333 (2004).
- [13] Y.W. Wang, L. Zhang, S. Li, P. Jena, *J. Phys. Chem. C*, **113**, 9210 (2009).
- [14] V. Stengl, S. Bakardjieva, N. Murafa. *Mater. Chem. Phys.* **114**, 217 (2009).
- [15] B.S. Rao, B.R. Kumar, V.R. Reddy, T.S. Rao, G.V. Chalapathi., *Chalcogenide Letters* **9**, 517 (2012).
- [16] A.A. Saif, Z. Ajamal, Z. Sauli, P. Poopalan. *Mat Sc. (medziagotyra)* **17**, 186 (2011).
- [17] T. Prodromakis, C. Papavassiliou, *Appl. Surf. Sci.*, **255**, 6989 (2009).
- [18] A. Azam, A.S. Ahmad, M. Chaman, A.H. Naqvi, *J. Appl. Phys.*, **108**, 094329 (2010).

*Corresponding author: oalhartomy@hotmail.co.uk